Ieee Transactions On Geoscience And Remote Sensing
March 2014, Volume 52, Issue 3, Pages 1879-1891
http://dx.doi.org/10.1109/TGRS.2013.2256362

Vegetation Height Estimation Precision With Compact PolInSAR and Homogeneous Random Volume Over Ground Model

Arnaubec Aurelien[1, 2], Roueff Antoine[2], Dubois-Fernandez Pascale C.[3], Refregier Philippe[2]

[1] Off Natl Etud & Rech Aerosp, Imager Radar & Testing Unit, Dept Electromagnetism & Radar, F-13661 Salon De Provence, France.
[2] Aix Marseille Univ, CNRS, Inst Fresnel, UMR 7249, F-13013 Marseille, France.
[3] Off Natl Etud & Rech Aerosp, Dept Electromagnetism & Radar, F-13661 Salon De Provence, France.

*: Corresponding authors : email addresses : aurelien.arnaubec@centrale-marseille.fr ; antoine.roueff@centrale-marseille.fr ; pascale.dubois-fernandez@onera.fr ; philippe.refregier@fresnel.fr

Abstract:

Analyzing the precision of vegetation height estimation with compact (i.e., single transmit instead of dual transmit) polarimetric interferometric synthetic aperture radar (PolInSAR) with the homogeneous random volume over ground model can help justify the use of this type of radar rather than using the full PolInSAR. However, since compact PolInSAR provides less information than full PolInSAR, a loss of precision in the vegetation height estimation is expected, which can depend on the single transmit polarization. The adaptation of the Cramer-Rao bound (CRB) derived for full PolInSAR in our earlier work to compact PolInSAR measurement provides a general methodology to characterize this loss of precision. Indeed, the CRB is a lower bound of the variance of unbiased estimators that does not depend on the choice of a particular estimation method. We illustrate this methodology for P-band measurements with three synthetic examples chosen for their variability of polarimetric responses. For these examples, it is shown that there can exist a large set of transmit polarizations for which the loss of precision described by the CRB is small (smaller than a factor 2) although there also exist transmit polarizations for which the loss can be large (about a factor 100). This loss of precision is compared with the large dependency of the precision to the vegetation height estimation that can be observed with the vegetation height (more than a factor 100 in the precision described by the CRB) when all the other parameters of the vegetation, ground, and radar system are constant.

Keywords: Compact polarimetry (CP) ; Cramer–Rao bound (CRB) ; polarimetric SAR interferometry (PolInSAR) ; random volume over ground (RVoG) model

1. Introduction

Full Polarimetric Interferometric Synthetic Aperture Radar (PolInSAR) can be used to estimate vegetation height with Random Volume over Ground model (RVoG) [2], [3], [4], [5], [6], [7], [8], [9], [10], [11] and different estimation techniques have been developed [4], [5], [6], [7], [11]. However, due

to constraints imposed by space-borne missions, it has been proposed to analyze if compact PolInSAR [9], [12] and PolSAR [13], [14], [15], [16] could be an alternative to full polarimetric systems. With compact PolInSAR systems [13], [14], [9], [15], [12], [16], two compact PolSAR datasets are measured from two different locations. For each compact PolSAR dataset, the scene is illuminated with only one polarization instead of two orthogonal polarizations that are transmitted sequentially with full PolSAR approaches. At the reception, the two orthogonal linear polarizations (horizontal H and vertical V) are received. Since each compact PolSAR dataset corresponds to two scalar SAR images obtained from two different locations, a compact PolInSAR dataset finally results in four complex scalar images instead of six with full PolInSAR dataset (assuming the reciprocity principle). Hence, compact PolInSAR leads to a loss of information in comparison with full PolInSAR and this loss is expected to be a function of the single transmit (i.e. emitted) polarization state. It has been shown in [1] from numerical simulations that the Cramer-Rao Bound (CRB) can be useful to analyze the vegetation height estimation precision obtained with full PolInSAR and the homogeneous RVoG vegetation model. Indeed, the CRB provides a lower bound to the variance of any unbiased estimator. In this article, we propose to adapt this approach [1] in order to analyze the CRB

obtained as a function of the transmit polarization of a compact PolInSAR system. Such an analysis allows one to rigorously characterize the loss of precision that results from using a compact instead of full PolInSAR system. Indeed, such a characterization is independent of a particular estimation method of the vegetation or of the ground height and only depends on the PolInSAR response model. As a consequence, the CRB analysis allows one to know if a poor precision in the estimation of these parameters results from a lack of information of the analyzed data. We illustrate this aspect with numerical simulations in which a simple adaptation of the estimation method introduced by Cloude and Papathanassiou [6] to compact PolInSAR is applied on synthetic examples. Each example is assumed to follow an RVoG model, and thus is characterized by a vegetation and ground height, and coherency matrices of the volume and of the ground. Furthermore, this RVoG model is restricted to media with azimuthal symmetry on the volume and reflection symmetry on the ground [17]. It is shown that this simple technique can lead for the considered examples to an estimation variance of compact PolInSAR close to the CRB for sufficiently large set of pixels of the analyzed area. We also derive a simple method to evaluate the minimum size under which the estimation is surely not efficient.

In the following, we illustrate the usefulness of the CRB methodology with three examples. These examples have not been selected in order to describe particular forests, but to illustrate the variability of results that can be obtained. In particular, we show that the precision can strongly vary with the transmit polarization. Although optimal transmit polarizations (i.e. that minimize the CRB) can vary with the vegetation height when the other RVoG parameters are fixed, efficient trade-off between precision and system implementation complexity have been obtained with a priori fixed transmit polarizations for the considered examples of this paper. Nevertheless, it appears important to precisely characterize the influence of the transmit polarization for each new physical situation. Indeed, different behaviors may be obtained with different characteristics of the vegetation properties, which can modify the performance of the considered transmit polarizations. This variability of behaviors confirms the importance of using the CRB to analyze the precision that can be expected for vegetation height estimation.

II. Background on PolInSAR and homogeneous RVoG model

A. PolInSAR measurements

The basic principles of single baseline full PolInSAR configuration consists of two antennas so that each antenna corresponds to a different location. The transmit antennas illuminate the scene with two orthogonal polarization states and the backscattered field is measured for each antenna along two orthogonal polarization states respectively denoted H and V [18]. Denoting also H and V the orthogonal transmit polarization states, the measured signal for antenna p (with $p = 1, 2$) is S_p^{HH}, S_p^{HV} when the transmit polarization is H and S_p^{VH}, S_p^{VV} when the transmit polarization is V. Assuming that the reciprocity principle holds leads to $S_p^{VH} = S_p^{HV}$. As a consequence, a full PolInSAR acquisition corresponds to the measurements S_1^{HH}, S_1^{HV}, S_1^{VV}, S_2^{HH}, S_2^{HV}, S_2^{VV}. Using $\boldsymbol{u}_p = \left[S_p^{HH},\ \sqrt{2}\ S_p^{HV},\ S_p^{VV}\right]^T$ where ^{T} is the transpose operator, the vector of measurements can be written $\boldsymbol{k} = \left[\boldsymbol{u}_1^T,\ \boldsymbol{u}_2^T\right]^T$.

In SAR datasets, due to the presence of fully developed speckle [19], the backscattering vector $\boldsymbol{k}$ is assumed to be a realization of a random vector with a zero mean complex circular Gaussian probability density. The random vector $\boldsymbol{k}$ is then characterized by its covariance matrix $\boldsymbol{\Upsilon}$

$$\boldsymbol{\Upsilon} = \langle \boldsymbol{k}\boldsymbol{k}^\dagger \rangle = \begin{bmatrix} \boldsymbol{T}_1 & \boldsymbol{\Omega} \\ \boldsymbol{\Omega}^\dagger & \boldsymbol{T}_2 \end{bmatrix} \tag{1}$$

where † is the Hermitian operator and $\langle\ \rangle$ is the statistical average. This 6×6 covariance matrix $\boldsymbol{\Upsilon}$ can be estimated in homogeneous regions where the measurements are identically distributed (i.e. so that the $\boldsymbol{k}$ vectors for each pixel are distributed with the same probability density function). Furthermore, $\boldsymbol{\Upsilon}$ is a simple function of the covariance matrices $\boldsymbol{T}_p = \langle \boldsymbol{u}_p \boldsymbol{u}_p^\dagger \rangle$ defined for each antenna p and of the interferometric coherency matrix $\boldsymbol{\Omega} = \langle \boldsymbol{u}_1 \boldsymbol{u}_2^\dagger \rangle$ defined between antennas number 1 and 2.

With compact PolInSAR mode, a single polarisation is transmitted, and the compact scattering response can be derived from the full PolInSAR model. The Jones vector $\boldsymbol{J}(\psi, \chi) = [J_1(\psi, \chi), J_2(\psi, \chi)]^T$ of the compact transmit polarization corresponds to an elliptic polarization state (see [20, 38] or [21, 16]) with orientation ψ and ellipticity χ that can be written

$$\begin{aligned} J_1(\psi, \chi) &= \cos\psi \cos\chi - i \sin\psi \sin\chi \\ J_2(\psi, \chi) &= \sin\psi \cos\chi + i \cos\psi \sin\chi \end{aligned} \tag{2}$$

where $i^2 = -1$. For antenna p, the compact system response $\tilde{\boldsymbol{u}}_p(\psi,\chi) = [\tilde{S}_p^H(\psi,\chi), \tilde{S}_p^V(\psi,\chi)]^T$ to the incident polarization $\boldsymbol{J}(\psi,\chi)$ can be deduced from the full polarimetric response (see [20], [21]) with

$$\begin{bmatrix} \tilde{S}_p^H(\psi,\chi) \\ \tilde{S}_p^V(\psi,\chi) \end{bmatrix} = \begin{bmatrix} S_p^{HH} & S_p^{HV} \\ S_p^{HV} & S_p^{VV} \end{bmatrix} \boldsymbol{J}(\psi,\chi) \tag{3}$$

then

$$\tilde{\boldsymbol{u}}_p(\psi,\chi) = \boldsymbol{A}(\psi,\chi)\ \boldsymbol{u}_p \tag{4}$$

with

$$\boldsymbol{A}(\psi,\chi) = \begin{bmatrix} J_1(\psi,\chi) & \frac{J_2(\psi,\chi)}{\sqrt{2}} & 0 \\ 0 & \frac{J_1(\psi,\chi)}{\sqrt{2}} & J_2(\psi,\chi) \end{bmatrix} \tag{5}$$

which leads to the covariance matrices

$$\langle \tilde{\boldsymbol{u}}_p(\psi,\chi)\tilde{\boldsymbol{u}}_q(\psi,\chi)^\dagger \rangle = \boldsymbol{A}(\psi,\chi)\langle \boldsymbol{u}_p\boldsymbol{u}_q^\dagger \rangle \boldsymbol{A}(\psi,\chi)^\dagger \tag{6}$$

with $p = 1,2$ and $q = 1,2$. The compact covariance matrices $\widetilde{\boldsymbol{T}}_p(\psi,\chi) = \langle \tilde{\boldsymbol{u}}_p(\psi,\chi)\tilde{\boldsymbol{u}}_p(\psi,\chi)^\dagger \rangle$ with $p = 1,2$ and the compact interferometric coherency matrix $\widetilde{\boldsymbol{\Omega}}(\psi,\chi) = \langle \tilde{\boldsymbol{u}}_1(\psi,\chi)\tilde{\boldsymbol{u}}_2(\psi,\chi)^\dagger \rangle$ can thus be easily deduced from the full covariance matrices $\boldsymbol{T}_p$ and from the full interferometric coherency matrix $\boldsymbol{\Omega}$.

B. Homogeneous RVoG Model

Although it has been shown that more precise scatterer repartition can be estimated with multibaseline configurations [22], [23], [24] than with single baseline systems, these last configurations also have some advantages and need to be characterized. Indeed, single baseline systems are simpler than multibaseline systems and we propose in this paper to investigate the additional simplification obtained with compact polarimetry. The estimation is then based on a simple model for the compact PolInSAR response that corresponds to the response of a Random Volume over a Ground (RVoG)[2], [3]. The ground response describes the backscattering of the wave by scatterers located at the ground level and can include a part of the ground-tree interaction responses, which can introduce double bounces. The volume response occurs in the vegetation which is described with statistically independent scatterers. Several hypotheses are made in this paper in order to simplify the vegetation model. The first one is that the scatterers are randomly located with a constant concentration along the vertical direction, which corresponds to a homogenous model. The second one consists in considering isotropic volume response, which corresponds to randomly oriented scatterers with an isotropic distribution. This assumption implies that if the transmit polarization is rotated by a fixed angle then the polarization state of the wave backscattered by the volume is also rotated by the same angle.

In this case, a simple parametric description of the matrices $\boldsymbol{T}_p$ and $\boldsymbol{\Omega}$ can be obtained. Let h_v denotes the vegetation height that has to be estimated. With full polarimetry and homogeneous RVoG model, the vegetation (or volume) and the ground responses are respectively described by the 3×3 Hermitian polarimetric coherency matrices $\boldsymbol{T}_{vol}$ and $\boldsymbol{T}_{gro}$ and by the mean extinction σ_v of the vegetation. The acquisition configuration is characterized by the incident angle θ and the height sensitivity k_z which are defined by the acquisition geometry. As explained in [25], $k_z = \frac{4\pi B_\perp}{\lambda R \sin\theta}$ where $B_\perp$ is the perpendicular baseline, R the range and λ the free space wavelength.

The hypothesis of homogenous RVoG model implies that the different volume layers are characterized by the same coherency matrix $\boldsymbol{T}_{vol}$ and it can then be shown [2], [3], [6] that the RVoG model can be written in that case

$$\begin{array}{c} \boldsymbol{T}_1 = \boldsymbol{T}_2 = I_1\boldsymbol{T}_{vol} + a\boldsymbol{T}_{gro} \\ \boldsymbol{\Omega} = e^{i\phi_g}\left(I_2\boldsymbol{T}_{vol} + a\boldsymbol{T}_{gro}\right) \end{array} \tag{7}$$

where, neglecting the thermal noise, I_1, I_2 and ϕ_g can be written

$$I_1 = \frac{1-e^{-\alpha h_v}}{\alpha} \quad I_2 = \frac{e^{ik_z h_v} - e^{-\alpha h_v}}{ik_z + \alpha} \quad \phi_g = k_z z_g \tag{8}$$

with $a = e^{-\alpha h_v}$, $\alpha = \frac{2\sigma_v}{\cos\theta}$ and where z_g is the relative ground height after removal of the flat earth phase contribution[25].

It has been shown [18], [26] that the homogeneous RVoG model can be used to estimate the vegetation height h_v with P-band single baseline configuration [8], [9]. In that case, the a priori knowledge of the attenuation parameter σ_v is required. In this paper, the value of σ_v measured in [8] and reported in Table I, will be considered. With such an a priori knowledge, the parameters h_v, $\boldsymbol{T}_{vol}$, $\boldsymbol{T}_{gro}$ and the ground phase ϕ_g can be estimated.

C. CRB for full PolInSAR and homogeneous RVoG model

It has been shown in [1] that the CRB can be useful to characterize the estimation precision in the scope of the homogeneous RVoG model with full PolInSAR. Let us recall useful statistical notions for this paper that have also been presented in [1]. For this purpose,

let $t_{vol,1}, t_{vol,2}, ..., t_{vol,9}$ and $t_{gro,1}, t_{gro,2}, ..., t_{gro,9}$ denote respectively the 9 unknown real coefficients of $\boldsymbol{T}_{vol}$ and $\boldsymbol{T}_{gro}$. With this notation, each complex coefficient corresponds to two real parameters. Furthermore, let $\mathcal{K} = \{\boldsymbol{k}_1, \boldsymbol{k}_2, ..., \boldsymbol{k}_N\}$ denotes the N backscattered measured signals used to get the estimation $\widehat{h}_v(\mathcal{K})$ of h_v. More generally, if $\boldsymbol{\nu} = [h_v, \phi_g, t_{vol,1}, t_{vol,2}, ..., t_{gro,9}]^T$ denotes the vector of unknown parameters, each of these 20 parameters ν_j can be estimated with $\mathcal{K}$ leading to 20 estimators $\widehat{\nu}_j(\mathcal{K})$. The estimator $\widehat{\nu}_j(\mathcal{K})$ is unbiased if the statistical average $\langle\widehat{\nu}_j(\mathcal{K})\rangle$ over the different possible realizations of $\mathcal{K}$ is equal to the true value ν_j^0 of the parameter. Otherwise the bias is defined by $b[\widehat{\nu}_j(\mathcal{K})] = \langle\widehat{\nu}_j(\mathcal{K})\rangle - \nu_j^0$. The precision of an unbiased estimator can be characterized with its variance $var[\widehat{\nu}_j(\mathcal{K})] = \langle[\widehat{\nu}_j(\mathcal{K}) - \langle\widehat{\nu}_j(\mathcal{K})\rangle]^2\rangle$ that measures the dispersion of the estimated values around the mean value.

A minimal bound of the variance of $\widehat{\nu}_j(\mathcal{K})$ is obtained with the CRB and such an approach has been developed in [1] for full PolInSAR with the RVoG model. The Cramer Rao lower bound specifies [1], [27] that any unbiased estimator satisfies the following inequality for any vector $\boldsymbol{a} \in \mathbb{R}^D$ [27] where D is the number of unknown real parameters:

$$\boldsymbol{a}^T \boldsymbol{\Sigma} \boldsymbol{a} \geq \boldsymbol{a}^T (\boldsymbol{I}_F)^{-1} \boldsymbol{a} \tag{9}$$

with $\boldsymbol{\Sigma} = \langle \delta\widehat{\boldsymbol{\nu}} \left(\delta\widehat{\boldsymbol{\nu}}\right)^T \rangle$, $\delta\widehat{\boldsymbol{\nu}} = \widehat{\boldsymbol{\nu}}(\mathcal{K}) - \boldsymbol{\nu}^0$, $[\widehat{\boldsymbol{\nu}}(\mathcal{K})]_j = \widehat{\nu}_j(\mathcal{K})$, $[\boldsymbol{\nu}^0]_j = \nu_j^0$ and where $\boldsymbol{I}_F$ is the Fisher information matrix of size $D \times D$ defined with $[\boldsymbol{I}_F]_{i,j} = -\langle \frac{\partial^2}{\partial\nu_i \partial\nu_j} \log P(\mathcal{K}|\boldsymbol{\nu}^0) \rangle$ where $P(\mathcal{K}|\boldsymbol{\nu}^0)$ is the probability density function of observing $\mathcal{K}$ when the parameter is $\boldsymbol{\nu}^0$. When the N measurements of the PolInSAR dataset are statistically independent and identically distributed with a zero mean complex circular Gaussian density, the Fisher information matrix $\boldsymbol{I}_F$ can be obtained using the Slepian-Bang formula [28]

$$[\boldsymbol{I}_F]_{j,\ell} = N \text{ tr} \left(\boldsymbol{\Upsilon}^{-1} \frac{\partial \boldsymbol{\Upsilon}}{\partial \nu_j} \boldsymbol{\Upsilon}^{-1} \frac{\partial \boldsymbol{\Upsilon}}{\partial \nu_\ell} \right) \tag{10}$$

where tr is the trace operator. Equation (9) leads in particular to $var[\widehat{\nu}_j(\mathcal{K})] \geq \left[(\boldsymbol{I}_F)^{-1}\right]_{j,j}$ which corresponds to a minimal bound for the variance of any unbiased estimator of ν_j. An unbiased estimator is efficient if it reaches the bound, i.e. if the inequality of Eq.(9) becomes an equality [27]. In this case, the covariance matrix $\boldsymbol{\Sigma}$ is equal to the inverse of the Fisher information matrix and the non-diagonal elements of $(\boldsymbol{I}_F)^{-1}$ correspond to the covariance values of the different estimations. More precisely, for such efficient estimators, the covariance between the fluctuations of the estimators are equal to $cov(\widehat{\nu}_j, \widehat{\nu}_\ell) = \langle[\widehat{\nu}_j(\mathcal{K}) - \langle\widehat{\nu}_j(\mathcal{K})\rangle] [\widehat{\nu}_\ell(\mathcal{K}) - \langle\widehat{\nu}_\ell(\mathcal{K})\rangle]\rangle = \left[(\boldsymbol{I}_F)^{-1}\right]_{j,\ell}$.

In order to compute the Fisher matrix $\boldsymbol{I}_F$, the terms $\partial\boldsymbol{\Upsilon}/\partial\nu_j$ have to be obtained from the derivatives of Eq. (7) with respect to h_v, ϕ_g, and the elements of $\boldsymbol{T}_{vol}$ and $\boldsymbol{T}_{gro}$ as detailed in [1].

III. Height precision analysis with the CRB for compact PolInSAR

A. CRB for compact PolInSAR and RVoG model

The CRB analyzed in [1] for full PolInSAR systems can be adapted to compact PolInSAR measurements, which allows one to easily compute the CRB for different values of the RVoG parameters. Using Eqs. (6), (7) and (8), it is easy to obtain the response of compact PolInSAR systems with the RVoG model. Indeed, let $\widetilde{\boldsymbol{\Upsilon}}$ denote the 4×4 covariance matrix of the 4 dimensional measured vector $\tilde{\boldsymbol{k}}(\psi, \chi) = \left[\tilde{\boldsymbol{u}}_1(\psi, \chi)^T,\ \tilde{\boldsymbol{u}}_2(\psi, \chi)^T\right]^T$. With the same assumptions of homogeneous RVoG model as for full polarimetry, the covariance matrix can be written

$$\widetilde{\boldsymbol{\Upsilon}} = \begin{bmatrix} \widetilde{\boldsymbol{T}}_1 & \widetilde{\boldsymbol{\Omega}} \\ \widetilde{\boldsymbol{\Omega}}^\dagger & \widetilde{\boldsymbol{T}}_2 \end{bmatrix} \tag{11}$$

with

$$\begin{aligned} \widetilde{\boldsymbol{T}}_j &= I_1 \widetilde{\boldsymbol{T}}_{vol} + a \widetilde{\boldsymbol{T}}_{gro} \\ \widetilde{\boldsymbol{\Omega}} &= e^{i\phi_g} \left(I_2 \widetilde{\boldsymbol{T}}_{vol} + a \widetilde{\boldsymbol{T}}_{gro} \right) \end{aligned} \tag{12}$$

where $\widetilde{\boldsymbol{T}}_{vol} = \widetilde{\boldsymbol{T}}_{vol}(\psi, \chi)$ and $\widetilde{\boldsymbol{T}}_{gro} = \widetilde{\boldsymbol{T}}_{gro}(\psi, \chi)$ can be obtained for each ψ, χ values with Eq. (6) as follow:

$$\widetilde{\boldsymbol{T}}_m = \boldsymbol{A}(\psi, \chi) \boldsymbol{T}_m \boldsymbol{A}(\psi, \chi)^\dagger \tag{13}$$

where $m = vol, gro$. These matrices are unknown since $\boldsymbol{T}_{gro}$ and $\boldsymbol{T}_{vol}$ are unknown.

Thus, let $\tilde{t}_{vol,1}, \tilde{t}_{vol,2}, \tilde{t}_{vol,3}, \tilde{t}_{vol,4}$ and $\tilde{t}_{gro,1}, \tilde{t}_{gro,2}, \tilde{t}_{gro,3}, \tilde{t}_{gro,4}$ denote the 8 unknown real coefficients of the Hermitian 2×2 matrices $\widetilde{\boldsymbol{T}}_{vol}$ and $\widetilde{\boldsymbol{T}}_{gro}$, and let us introduce the vector of unknown parameters $\boldsymbol{\eta} = [h_v, \phi_g, \tilde{t}_{vol,1}, \tilde{t}_{vol,2}, ..., \tilde{t}_{gro,4}]^T$. From the measurement set $\mathcal{K}$ obtained in compact configuration, each η_j with $j = 1, 2, .., 10$ can be estimated and these estimations will be noted $\widehat{\eta}_j(\mathcal{K})$. The Fisher information for transmit polarization of orientation and ellipticity (ψ, χ) is then given by [28], [1]

$$\left[\widetilde{\boldsymbol{I}}_F(\psi, \chi)\right]_{j,\ell} = N \text{ tr} \left(\frac{\partial \widetilde{\boldsymbol{\Upsilon}}}{\partial \eta_j} \widetilde{\boldsymbol{\Upsilon}}^{-1} \frac{\partial \widetilde{\boldsymbol{\Upsilon}}}{\partial \eta_\ell} \widetilde{\boldsymbol{\Upsilon}}^{-1} \right) \tag{14}$$

which has to be evaluated with $\widetilde{\boldsymbol{T}}_{vol}(\psi,\chi)$ and $\widetilde{\boldsymbol{T}}_{gro}(\psi,\chi)$ obtained for each ψ,χ values with Eq. (13).

B. Influence of the transmit polarization

In the following, the precision described by the CRB of the vegetation height estimation of compact PolInSAR is illustrated with three examples that are described in Table I. For each set of parameters in Table I, the CRB is computed in full configuration with Eq.(7) and Eq.(10) and the ones in compact configuration with Eq.(12) and Eq.(14). The considered experimental context corresponds to P-band PolInSAR systems, which have been used for example with the ONERA RAMSES system (see for example [10] for the Pyla 2004 campaign) or with the SETHI system (see for example [29] for the TropiSAR campaign). Although these examples can be obtained from estimations with P-band PolInSAR measurements [10], [29] when the volume and ground coherency matrices are constrained using symmetry properties[17], they have not been selected for their representativity of real situations but to illustrate the variability of behaviors that can be encountered. Note that in Table I, the energy of the ground on HH is higher than on VV because the coherency matrix $\boldsymbol{T}_{gro}$ is actually the sum of two contributions: the ground backscattering and the ground-to-truck interaction (double bounce) which are both located at the same height z_g.

Let $CRB_F(h_v)$ and $CRB_C(h_v)$ denote respectively the CRB of h_v with full and compact PolInSAR. These quantities are respectively equal to $\left[\boldsymbol{I}_F^{-1}\right]_{1,1}$ and to $\left[\widetilde{\boldsymbol{I}}_F(\psi,\chi)^{-1}\right]_{1,1}$. It is expected that $CRB_F(h_v) \leq CRB_C(h_v)$ since the compact PolInSAR measurement is a subset of the full PolInSAR measurement. The comparison of compact and full PolInSAR for the estimation of h_v can be obtained with $\rho(\psi,\chi) = CRB_C(h_v)/CRB_F(h_v)$. Indeed, the ratio $\rho(\psi,\chi)$ characterizes the relative increase of the CRB using a compact instead of a full PolInSAR system. Furthermore, it can be noticed that the same precision is obtained with an unbiased efficient estimator if the number of measurements N_C and N_F of respectively a compact and a full PolInSAR system satisfy $N_C = \rho(\psi,\chi)N_F$. As a consequence, this ratio $\rho(\psi,\chi)$ also characterizes the loss of spatial resolution for vegetation height estimation for a fixed vegetation height estimation precision with unbiased efficient estimators.

The ratio $\rho(\psi,\chi)$ is shown in Figure 1 as a function of ψ and χ for the two first examples of Table I. For these figures, the vertical axis ψ has been regularly sampled between 0 and π with 101 values whereas the horizontal axis χ has been regularly sampled between $-\pi/4$ and $\pi/4$ with 51 values. For Ex 1, the CRB of h_v with full polarimetry (i.e. $CRB_F(h_v)$) is approximately equal to 6 m^2 for a sample size $N = 100$. In other words, 600 pixels are needed to get a precision of one meter for efficient estimators. Furthermore, for Ex 1, and with the considered sampling on ψ and χ, the obtained minimal value ρ_{min} of $\rho(\psi,\chi)$ is 1.09, while its maximal value ρ_{max} is 143. The polarization states that correspond to these extrema are also shown in Figure 1. For Ex 2, the considered sampling leads to $\rho_{min} \simeq 1.63$, $\rho_{max} \simeq 16$ and $CRB_F(h_v) \simeq 25$ m^2 for $N = 100$. It can also be observed on Ex 1 and Ex 2 that $\rho(\psi,\chi)$ have narrow maxima and that there is a non-negligible dependence of $CRB_C(h_v)$ on the transmit polarization (ψ,χ).

The values of $\rho(\psi,\chi)$ for Ex 1, 2 and 3 for four particular transmit polarizations that have been discussed in the literature [13], [14], [9] and for the best transmit polarization P_B that minimizes $\rho(\psi,\chi)$ and the worse P_W that maximizes $\rho(\psi,\chi)$ are reported in Table II. The four particular transmit polarizations correspond to linear Horizontal ($\psi = 0, \chi = 0$) denoted P_H, linear Vertical ($\psi = \pi/2, \chi = 0$) denoted P_V, linear oriented at $\pi/4$ ($\psi = \pi/4, \chi = 0$) denoted $P_{\pi/4}$ and Circular transmit polarization ($\psi \in [0,\pi], \chi = \pm\pi/4$) denoted P_C. With Ex 1, the value of $\rho(\psi,\chi)$ for transmit polarization P_H and $P_{\pi/4}$ are close to the optimal one. The value of $\rho(\psi,\chi)$ for transmit polarization P_C (which, for space-borne mission, presents the advantage of being Faraday rotation insensitive) is approximately three times larger than the optimal one and the double of the one obtained with $P_{\pi/4}$. Finally, the value of $\rho(\psi,\chi)$ obtained with linear Vertical polarization P_V is close to the worst value. With Ex 2 the situation is slightly different. Indeed, the transmit polarization P_V leads for this example to CRB values much better than the worst CRB value. For this example, P_C and $P_{\pi/4}$ still lead to an increase of the CRB smaller than three times the value of the minimal compact CRB value (i.e. with P_B). With Ex 3 the hierarchy between the polarization states is the same as for Ex 1.

The results of Table II show, on the analyzed examples, that the horizontal linear and $\pi/4$ linear transmit polarizations have provided low CRB in-

	Ex 1	Ex 2	Ex 3
k_z	0.141 m^{-1}	0.0783 m^{-1}	0.222 m^{-1}
θ	0.948 rad	0.977 rad	0.89 rad
σ_v	0.0345 m^{-1}	0.0345 m^{-1}	0.0345 m^{-1}
$\boldsymbol{T}_{gro}$	$\begin{matrix} 17.3 & 0 & 0.45-2.1i \\ 0 & 6.5 & 0 \\ 0.45+2.1i & 0 & 9.25 \end{matrix}$	$\begin{matrix} 89.5 & 0 & 15.6-23.2i \\ 0 & 31.8 & 0 \\ 15.6+23.2i & 0 & 85.9 \end{matrix}$	$\begin{matrix} 43.4 & 0 & -9.65-10i \\ 0 & 0.3 & 0 \\ -9.65+10i & 0 & 4.75 \end{matrix}$
$\boldsymbol{T}_{vol}$ (m^{-1})	$\begin{matrix} 0.32 & 0 & 0.07 \\ 0 & 0.25 & 0 \\ 0.07 & 0 & 0.32 \end{matrix}$	$\begin{matrix} 0.095 & 0 & 0.025 \\ 0 & 0.07 & 0 \\ 0.025 & 0 & 0.095 \end{matrix}$	$\begin{matrix} 0.795 & 0 & 0.225 \\ 0 & 0.57 & 0 \\ 0.225 & 0 & 0.795 \end{matrix}$
z_g	-2.7 m	-5.2 m	0 m
h_v in III-B	25 m	20 m	23.3 m
h_v in III-C,D	varies between 0 and 44 m	varies between 0 and 27 m	varies between 0 and 60 m
h_v in IV-B	14.6 m	not considered	23,3 m

TABLE I

FULL POLARIMETRY PARAMETER SETS FOR THREE EXAMPLES WITH $\boldsymbol{T}_{gro}$ AND $\boldsymbol{T}_{vol}$ IN LEXICOGRAPHIC BASIS TO BE USED FOR NUMERICAL SIMULATIONS. NOTE THAT THE VALUES OF h_v CHANGE BETWEEN SECTION III-B-C-D AND SECTION IV-B.

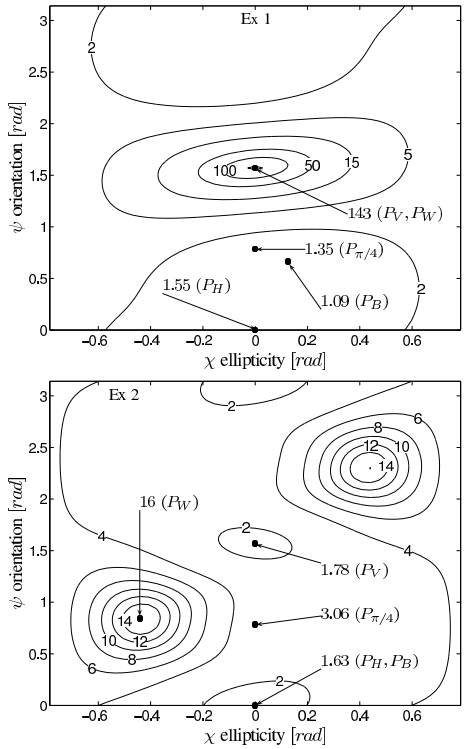

Fig. 1. The $\rho(\psi,\chi)$ ratio of the compact CRB with the full CRB as a function of the transmit polarization orientation and ellipticity parameters for the two first examples of Table I with $h_v = 25\ m$ for Ex 1 and $h_v = 20\ m$ for Ex 2. The compact CRB for polarizations P_H, P_V, $P_{\pi/4}$, P_B and P_W are also mentioned.

	P_B	P_H	P_V	$P_{\pi/4}$	P_C	P_W
Ex 1	1.09	1.55	143	1.35	2.8	143
Ex 2	1.63	1.63	1.78	3.06	4.5	16
Ex 3	1.06	1.4	99.1	1.13	1.89	99.1

TABLE II

VALUES OF $\rho(\psi,\chi)$ FOR THE THREE EXAMPLES IN FUNCTION OF THE TRANSMIT POLARIZATIONS P_B (BEST POLARIZATION, I.E. WHICH MINIMIZES THE CRB), P_H (HORIZONTAL POLARIZATION), P_V (VERTICAL POLARIZATION), $P_{\pi/4}$ ($\pi/4$ POLARIZATION), P_C (CIRCULAR POLARIZATION) AND P_W (WORSE POLARIZATION, I.E. WHICH MAXIMIZES THE CRB). FOR EX 1 WITH $h_v = 25\ m$, FOR EX 2 WITH $h_v = 20\ m$ AND FOR EX 3 WITH $h_v = 23.3\ m$.

crease in comparison to full polarimetry. However, Figure 1 demonstrates that the optimal transmit polarization can vary from one physical situation to another one. This difference of behaviors can result from differences of the intensities backscattered by the volume and by the ground, and also from differences of the polarimetric characteristics of the waves backscattered by each media. However, the difference of behaviors obtained with the horizontal and vertical transmit polarizations can be correlated with recent results obtained for PolSAR, PolInSAR and tomographic analysis [30], [31], [32], [17] and will be detailed later. Furthermore, the good performance of the $\pi/4$ linear transmit polarization can be interpreted for the analyzed examples as resulting of the ability of this polarization state to enhance the difference of polarization characteristics of the wave backscattered by the volume with the wave backscattered by the ground. Indeed, the ground response results from the contribution of the ground backscattering and of the ground-to-trunk interaction, which is anisotropic, while the volume is assumed isotropic.

Let us discuss more precisely these aspects. With compact PolInSAR, the polarimetric characteristics of the measured backscattered waves are the ones defined for electrical fields [33]: the main polarization state, which is the polarization state of the wave that contains the highest intensity, and the degree

of polarization of the wave, which is the normalized difference of the eigenvalue of the coherency matrix (i.e. the covariance matrix of the field). The polarization state can also be represented with a point in the Poincaré sphere [34], [33], [18]. The degree of polarization then corresponds to the distance of this point to the center of the sphere while the main polarization state corresponds to the direction defined by this point and the center of the sphere. For the considered examples the matrices $\boldsymbol{T}_{vol}$ have been constrained [6], [17] to describe isotropic media. Thus, the intensity of the wave backscattered by the volume is independent of the transmit polarization. Furthermore, if the transmit polarization is linear and is rotated by a fixed angle then the main polarization state of the backscattered wave is rotated by the same angle. As a result, the degrees of polarization noted respectively $\mathcal{P}_{vol}^{(H)}$ for horizontal, $\mathcal{P}_{vol}^{(V)}$ for vertical and $\mathcal{P}_{vol}^{(\pi/4)}$ for $\pi/4$ transmit polarizations are equal (i.e. $\mathcal{P}_{vol}^{(H)} = \mathcal{P}_{vol}^{(V)} = \mathcal{P}_{vol}^{(\pi/4)}$). Moreover, with linear transmit polarizations, the main polarization state of the wave backscattered by the volume remains equal to the transmit polarization state.

As mentioned above, the ground response is anisotropic (i.e. if a linear transmit polarization is rotated by a fixed angle then the main polarization state of the wave backscattered by the ground is not in general simply rotated by the same angle). However, if the transmit polarization is horizontal (respectively vertical) then the main polarization state of the wave backscattered by the ground is also horizontal (resp. vertical). This is no longer true with a linear polarization state oriented at $\pi/4$ since in that case the main polarization state of the wave backscattered by the ground is no longer a linear polarization state oriented at $\pi/4$. Thus, for vertical or horizontal transmit polarization, the difference of the polarization characteristics of the wave backscattered by the ground and by the volume is limited to the difference of their degrees of polarization, while for the linear polarization state oriented at $\pi/4$ the main polarization states of the backscattered waves are also different. The ability to estimate vegetation height is related to the ability to discriminate the ground and the volume responses [6]. This ability is function of the difference of the polarization characteristics of the waves backscattered by each media, which can be enhanced if their main polarization states are different. These difference of behaviors with the linear horizontal, vertical and $\pi/4$ transmit polarizations can be correlated with the results of Table II.

For circular transmit polarization, the wave backscattered by the volume has a lower degree of polarization than for a linear transmit polarization. This property may have an influence since if the degree of polarization $\mathcal{P}_{vol}^{(X)} = 0$ for a transmit polarization P_X, then the wave backscattered by the volume is totally depolarized and thus its difference of polarization characteristics with the wave backscattered by the ground mostly resort from the degree of polarization of this last wave and not from its main polarization state. These characteristics can be observed in Table III which presents, for the considered examples, the degrees of polarization of the wave backscattered by the volume $\mathcal{P}_{vol}^{(X)}$, by the ground $\mathcal{P}_{gro}^{(X)}$ and the ratio $R^{(X)} = Tr[\widetilde{\boldsymbol{T}}_{gro}^{(X)}]/Tr[\widetilde{\boldsymbol{T}}_{vol}^{(X)}]$ that is proportional to the intensity of the wave backscattered by the ground. This table also indicates whether the main polarization states of the wave backscattered by the volume and by the ground are identical.

The difference between the precision of the vegetation height estimation with the vertical or with the horizontal transmit polarization can be analyzed with the suggestion of different analysis [30], [31], [32] that $\langle|S^{HH}|^2\rangle \geq \langle|S^{VV}|^2\rangle \geq \langle|S^{HV}|^2\rangle$ and that $\langle S^{HH}S^{HV}\rangle \simeq \langle S^{VV}S^{HV}\rangle \simeq 0$ [17] for forest grounds. These relations have been confirmed with recent tomographic analysis such as [35], [36] and are consistant with the analyzed examples of this paper. In that case the difference of the polarization characteristics of the waves backscattered by the volume or by the ground can only depend of their degrees of polarization since, for both the vertical and the horizontal transmit polarizations, the main polarization state of the backscattered waves by both media are identical. However, the above inequalities imply that the degree of polarization of the wave backscattered by the ground with horizontal transmit polarization is greater than the one obtained with vertical transmit polarization (i.e. $|\langle|S_{gro}^{HH}|^2\rangle - \langle|S_{gro}^{HV}|^2\rangle|/(\langle|S_{gro}^{HH}|^2\rangle + \langle|S_{gro}^{HV}|^2\rangle) > |\langle|S_{gro}^{VV}|^2\rangle - \langle|S_{gro}^{HV}|^2\rangle|/(\langle|S_{gro}^{VV}|^2\rangle + \langle|S_{gro}^{HV}|^2\rangle)$), and is also greater than the degree of polarization of the wave backscattered by the volume. The difference of polarization characteristics of the waves backscattered by the ground and by the volume is thus higher with horizontal transmit polarization than with vertical transmit polarization.

It has been early noticed [6] that $\boldsymbol{T} = [\boldsymbol{T}_{vol}]^{-1}\boldsymbol{T}_{gro}$ is a relevant matrix and it reduces to $\widetilde{\boldsymbol{T}}^{(X)} =$

$[\widetilde{\boldsymbol{T}}_{vol}^{(X)}]^{-1}\widetilde{\boldsymbol{T}}_{gro}^{(X)}$ for compact PolInSAR. As detailed in [37], the difference of two waves can be characterized with two quantities that quantify the contrast between them. For the problem discussed in this paper, they corresponds to the two eigenvalues of $\widetilde{\boldsymbol{T}}^{(X)}$ noted $\lambda_1^{(X)}$ and $\lambda_2^{(X)}$ (or to a bijective transformation of these two quantities). It is interesting to report in Table III the normalized difference factors $A^{(X)} = \frac{|\lambda_1^{(X)}-\lambda_2^{(X)}|}{\lambda_1^{(X)}+\lambda_2^{(X)}}$, which has a simple physical interpretation. Indeed, if a linear transformation is applied to the received wave so that the wave backscattered by the volume is totally depolarized, this linear transformation also modifies the wave backscattered by the ground, but this wave usually remains partially polarized. The normalized difference factors $A^{(X)}$ is, in that case, equal to the degree of polarization of the wave backscattered by the ground after the linear transformation.

Finally, it is important to emphasize that although in the analyzed examples, a large value of $A^{(X)}$ is often an indication of a low compact PolInSAR CRB with transmit polarization P_X, it is not always the case (see in Table II and Table III for instance the CRB and $A^{(X)}$ for Ex 3 with circular and horizontal linear transmit polarizations). As previously mentioned, since there are actually two contrast parameters [37], the performance of the different transmit polarizations should not be interpreted considering only the polarization contrast $A^{(X)}$. The variation of the backscattered intensities ratio $R^{(X)}$ can also have an effect on the CRB. The large variation of this quantity for Ex 3 in comparison to Ex 1 and Ex 2 can explain the difference of behaviors for the interpretation with $A^{(X)}$. These results emphasize the importance of looking at the CRB which is further underlined in the next section where the dependency with the vegetation height is analyzed.

Ex		$\mathcal{P}_{vol}^{(X)}$	$\mathcal{P}_{gro}^{(X)}$	$R^{(X)}$	Diff$^{(X)}$	$A^{(X)}$
1	P_H	0.438	0.683	46.1 m	N	0.35
	P_V	0.438	0.48	28.1 m	N	0.05
	$P_{\pi/4}$	0.438	0.354	37.1 m	Y	0.36
	P_C	0.124	0.322	37.1 m	Y	0.28
2	P_H	0.462	0.698	810 m	N	0.35
	P_V	0.462	0.687	783 m	N	0.33
	$P_{\pi/4}$	0.462	0.379	797 m	Y	0.3
	P_C	0.077	0.225	797 m	Y	0.24
3	P_H	0.472	0.993	40.3 m	N	0.98
	P_V	0.472	0.939	4.54 m	N	0.84
	$P_{\pi/4}$	0.472	0.98	22.4 m	Y	0.99
	P_C	0.056	0.985	22.4 m	Y	0.99

TABLE III
DEGREES OF POLARIZATION $P_{vol}^{(X)}$ AND $P_{gro}^{(X)}$ OF, RESPECTIVELY, THE WAVE BACKSCATTERED BY THE VOLUME AND BY THE GROUND. RATIO OF INTENSITIES BACKSCATTERED BY THE GROUND AND BY THE VOLUME $R^{(X)}$, DIFF$^{(X)}$ INDICATES IF THE MAIN POLARIZATION STATES OF THE WAVE BACKSCATTERED BY THE VOLUME AND BY THE GROUND ARE DIFFERENT (Y) OR ARE IDENTICAL (N), NORMALIZED DIFFERENCE FACTORS $A^{(X)}$. THESE QUANTITIES ARE REPORTED FOR THE THREE EXAMPLES AND FOR 4 DIFFERENT TRANSMIT POLARIZATION, HORIZONTAL (P_H), VERTICAL (P_V), LINEAR ORIENTED AT $\pi/4$ ($P_{\pi/4}$) AND CIRCULAR (P_C).

C. Performance variations with the vegetation height

It is proposed in this section to analyze the CRB as a function of the vegetation height for different transmit polarizations. For that purpose, the methodology described in the previous section is applied for different values of h_v while the other parameters z_g, $\boldsymbol{T}_{vol}$ and $\boldsymbol{T}_{gro}$ are unchanged. For each example, the polarization has been optimized to determine P_W and P_B that respectively maximizes and minimizes $\rho(\psi,\chi)$ with the above mentioned sampling on ψ and χ for each h_v values sampled with a step of $\frac{e_a}{1000}$ (where e_a is the ambiguity height equal to $2\pi/k_z$). The values of the CRB of h_v as a function of h_v are reported in Figure 2 for transmit polarizations P_V, $P_{\pi/4}$ and P_C and for the transmit polarizations P_B and P_W for Ex 1 and Ex 3 of Table I. The full PolInSAR CRB is also reported on these figures.

It can be observed that the CRB of full and of compact PolInSAR measurements have globally the same shape. However, it is also clear for Ex 1 and Ex 3 that the CRB obtained with P_V is quite close to the worst transmit polarization P_W for all h_v and is significantly larger than with the other transmit polarizations. Furthermore, the $P_{\pi/4}$ polarization provides approximately the same CRB results as for the optimal one P_B for these examples. The performance obtained with the P_C (i.e. circular) polarization is slightly degraded in comparison with the one obtained with the $P_{\pi/4}$ and P_B polarizations.

It can also be observed with Ex 1 that there exists a vegetation height h_v^{loc} for which the CRB for compact and full PolInSAR presents a local minimal value. The CRB of both compact and full PolInSAR measurements drastically increases for h_v values larger than h_v^{loc}. Moreover, for the particular vegetation height h_v^{loc}, no significant difference of the CRB between the different considered transmit polarizations is observed. With Ex 1, when $N = 100$, the CRB for full PolInSAR measurement is approximately equal to 1.4 m^2 when $h_v = 6$ m, to 0.3 m^2 when $h_v = 16$ m and to 8 m^2 when $h_v = 26$ m. These differences are amplified with the worst transmit

polarization P_W. For instance with this example, approximately 2.10^3 pixels are needed to estimate the height of 30 meter trees with one meter precision with full PolInSAR and an efficient estimator, 3.10^3 pixels are needed with polarization $P_{\pi/4}$ while 3.10^5 pixels are necessary with the worst transmit polarizations (P_V and P_W).

The results obtained with Ex 3 have also been reported in order to show that a different behavior can be observed. However, the influence of h_v is still important since between $h_v \simeq 5\ m$ and $h_v \simeq 20\ m$ the CRB has increased by approximately a factor 10 for polarizations $P_{\pi/4}$ and P_C while the increase is about a factor 1000 for P_W and P_V.

We show in Figure 3 with Ex 2, the influence of optimizing the transmit polarization for different fixed h_v values. On the previous examples the results were presented for the transmit polarizations P_B that minimizes $\rho(\psi, \chi)$ for each h_v. In figure 3, the CRB is also shown when the transmit polarization is only optimized for $h_v = \frac{1}{11}\ e_a$ or $h_v = \frac{10}{11}\ e_a$ (respectively denoted $P_B\left(\frac{1}{11}e_a\right)$ and $P_B\left(\frac{10}{11}e_a\right)$) where $e_a = 2\pi/k_z$. Although the optimal transmit polarization is different for $h_v = \frac{1}{11}\ e_a$ and $h_v = \frac{10}{11}\ e_a$, we do not observe on this example a large degradation of the CRB if the CRB is optimized for a particular vegetation height. The CRB obtained with transmit polarization $P_{\pi/4}$ and P_W are also shown in this figure. Globally a similar behavior to the one of Ex 1 can be observed although the value of h_v^{loc} is different.

Finally, it can be noticed that the normalized difference of the eigenvalues of $[\widetilde{\boldsymbol{T}}_{vol}^{(X)}]^{-1}\widetilde{\boldsymbol{T}}_{gro}^{(X)}$ noted $A^{(X)}$ in Table III are smaller than 0.4 for Ex 1 and Ex 2 while they are larger than 0.8 for Ex 3 for which no local minima is observed.

D. Analysis of the local optimal vegetation height

It has been seen with Ex 1 and Ex 2 that there exists a vegetation height h_v^{loc} for which the CRB for compact and full PolInSAR measurements present a local minimal value and for which no significant difference of the CRB between the different considered transmit polarizations can be observed. In order to investigate this result, let us first analyze for Ex 1 the CRB on h_v when z_g is unknown or known, respectively denoted $CRB(h_v)$ and $CRB(h_v|z_g)$. The value of $CRB(h_v|z_g)$ is determined with the vector of unknown parameters $[h_v, \tilde{t}_{vol,1}, \tilde{t}_{vol,2}, ..., \tilde{t}_{gro,4}]^T$. This CRB is still obtained with Eq.(14) but now the size of the Fisher information matrix is 9×9. These CRB have been reported in Figure 4 for the

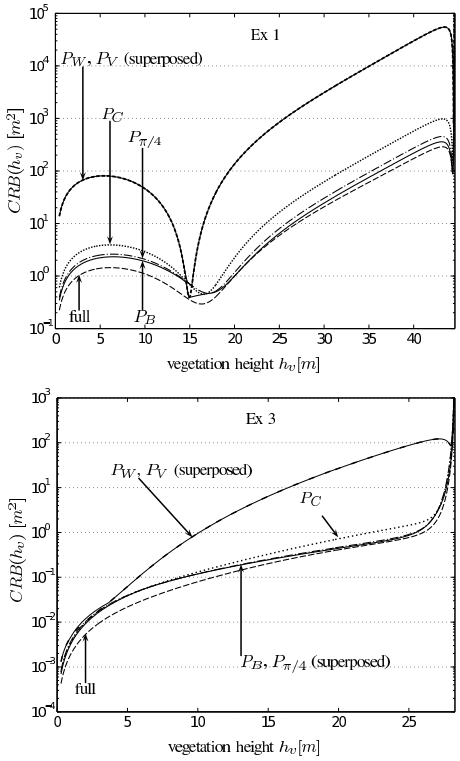

Fig. 2. Evolution of the CRB as a function of the vegetation height h_v for Ex 1 and Ex 3 of Table I and for fixed transmit polarization P_V, $P_{\pi/4}$, P_C, for the transmit polarization that minimizes (P_B) and maximizes (P_W) the CRB for each h_v and for full PolInSAR when the sample size is $N = 100$.

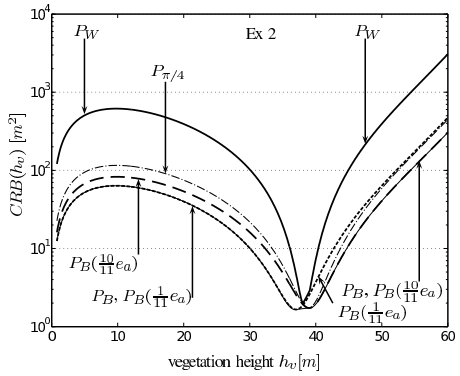

Fig. 3. Evolution of the CRB as a function of h_v for Ex 2 of Table I for the transmit polarization P_B that minimizes the CRB for each h_v, for the transmit polarization $P_B\left(\frac{1}{11}e_a\right)$ optimized for $h_v = \frac{1}{11}e_a$, $P_B\left(\frac{10}{11}e_a\right)$ optimized for $h_v = \frac{10}{11}e_a$, $P_{\pi/4}$ and P_W, and where $e_a = 2\pi/k_z$ and the sample size is $N = 100$.

vertical transmit polarization P_V. The CRB on the estimation of z_g denoted $CRB(z_g)$ is also reported. It can be seen that when z_g is known, there exists no sharp local minimum of $CRB(h_v|z_g)$. Furthermore, the knowledge of z_g decreases drastically the CRB on h_v on this example (i.e. $CRB(h_v|z_g) \ll CRB(h_v)$) and such an influence has already been reported for full PolInSAR measurements [38].

The correlation between the fluctuations of z_g and h_v that result from their estimation can be analyzed regarding their covariance. For efficient estimators, this covariance is equal to the off-diagonal element of the inverse of the Fisher information that corresponds to these variables, i.e. $cov(h_v, z_g) = \left[(\widetilde{\boldsymbol{I}}_F)(\psi,\chi)^{-1}\right]_{1,2}/k_z$. The normalized covariance $c_n(h_v, z_g) = cov(h_v, z_g)/\sqrt{CRB(h_v)CRB(z_g)}$, which varies necessarily between -1 and 1, has been shown for this example in Figure 4. It can be observed that $c_n(h_v, z_g)$ is positive for small h_v and negative for higher h_v. There also exists a value of h_v for which this normalized covariance is equal to 0. In that case, the fluctuations of the estimation of h_v are uncorrelated to the fluctuations of the estimation of z_g. The curve $CRB(h_v)$ has a local minimum approximately for this vegetation height and in that case, $CRB(h_v) \simeq CRB(h_v|z_g)$. It can thus be conjectured that, for this experimental configuration, most of the fluctuations of h_v when z_g is unknown correspond to transmission of the fluctuations of z_g to h_v through their correlation. A similar behavior has been observed with Ex 2 but not with Ex 3.

The behavior of the covariance between the estimations of h_v and z_g with finite size sets of pixels can be interpreted in the coherence diagram (i.e. representation of the coherence in the complex plane) as shown in Appendix A. In particular, at first order, the vegetation height for which there is no correlation between the estimation fluctuations of h_v and z_g corresponds to regions of coherence in the complex plane (after ground phase rotation) whose center is located on the circle of radius 1/2 and centered on the point of coordinates $(1/2, 0)$. Furthermore, let us introduce the volume only coherence

$$\gamma_V(h_v) = \frac{e^{ik_z h_v} - e^{-\alpha h_v}}{1 - e^{-\alpha h_v}} \frac{\alpha}{ik_z + \alpha} \tag{15}$$

which corresponds to I_2/I_1 of Eq. 8. It can be seen (see Appendix B) that, in the limit case where $|\gamma_V(h_v)| \simeq 1$ the circle of radius 1/2 and centered on $(1/2, 0)$ corresponds approximately to h_v values for which the same energy is scattered by the ground and by the volume. Note that this discussion on correlation between z_g and h_v is relevant for both compact and full configurations.

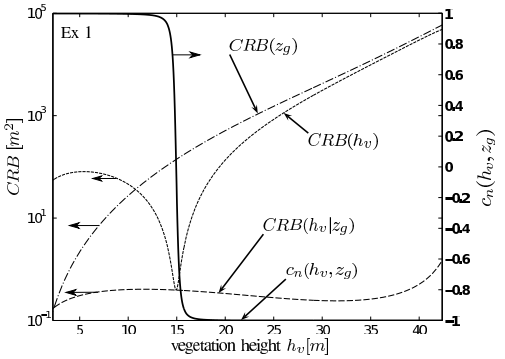

Fig. 4. CRB of h_v when z_g is known ($CRB(h_v|z_g)$), when z_g is unknown ($CRB(h_v)$) and CRB of z_g ($CRB(z_g)$) as a function of h_v when the sample size is $N = 100$ and for the vertical polarization (P_V) for Ex 1. Values correspond to the left axis. The normalized covariance $c_n(h_v, z_g)$ between h_v and z_g obtained with the Fisher information matrix is also reported (right axis).

IV. Efficiency analysis of a simple estimator for compact PolInSAR

A. Considered estimation method

Since there is no guarantee that any estimator is unbiased with a variance equal to the CRB, we propose in this section to discuss the efficiency of a simple estimation method. The considered method corresponds to a particular implementation of the Cloude and Papathanassiou estimator [6], [8] which has been adapted for compact PolInSAR measurements. This method has been used in [1] to discuss the CRB in the context of full PolInSAR measurements. The particular implementation for compact PolInSAR is based on the analysis of the region of coherence defined as the set of points in the complex plane obtained with

$$\gamma(\tilde{\boldsymbol{w}}) = \frac{\tilde{\boldsymbol{w}}^\dagger \widehat{\widetilde{\boldsymbol{\Omega}}} \tilde{\boldsymbol{w}}}{\sqrt{\tilde{\boldsymbol{w}}^\dagger \widehat{\widetilde{\boldsymbol{T}}}_1 \tilde{\boldsymbol{w}}\ \tilde{\boldsymbol{w}}^\dagger \widehat{\widetilde{\boldsymbol{T}}}_2 \tilde{\boldsymbol{w}}}} \tag{16}$$

where $\widehat{\widetilde{\boldsymbol{\Omega}}}$, $\widehat{\widetilde{\boldsymbol{T}}}_1$ and $\widehat{\widetilde{\boldsymbol{T}}}_2$ are the estimations of $\widetilde{\boldsymbol{\Omega}}$, $\widetilde{\boldsymbol{T}}_1$ and $\widetilde{\boldsymbol{T}}_2$ on a finite size set of N pixels and where $\tilde{\boldsymbol{w}}$ varies in the set of the six received polarizations that correspond to the following Jones vectors (in Lexicographic basis)

$$\left\{ \begin{bmatrix}1\\0\end{bmatrix}, \begin{bmatrix}0\\1\end{bmatrix}, \begin{bmatrix}1\\-1\end{bmatrix}, \begin{bmatrix}1\\1\end{bmatrix}, \begin{bmatrix}1\\j\end{bmatrix}, \begin{bmatrix}1\\-j\end{bmatrix} \right\} \tag{17}$$

A least squares line fit is then performed on the coherence points obtained with the previous Jones vectors. The ground phase ϕ_g is estimated with the intersections of this line with the unit circle centered on the point of coordinates $(0,0)$. Among the two obtained solutions, $\widehat{\phi_g}(\mathcal{K})$ is chosen to be the closest to the true value. Obviously, in real situations the true ground height is not available and other solutions have to be implemented [6], [5], [7], [8], [9]. The line is then rotated around the center of coordinates $(0,0)$ with an angle $-\widehat{\phi_g}(\mathcal{K})$ so that the point of coordinates $(0,1)$ belongs to the rotated line. When it exists, the intersection between the previous rotated line and $\gamma_V(h_v)$ defined with Eq. 15 leads to the estimated $\widehat{h_v}(\mathcal{K})$ value of h_v.

B. Numerical simulations and precision analysis

For each N value, a sample $\mathcal{K} = \{\boldsymbol{k}_1,\ \boldsymbol{k}_2,\ ...\boldsymbol{k}_N\}$ of random circular and complex vectors of covariance matrix $\boldsymbol{\Upsilon}$ has been generated and the vegetation height h_v and the ground phase ϕ_g have been estimated for 500 independent sample realizations, which allow one to estimate the bias $b[\widehat{h_v}(\mathcal{K})]$, $b[\widehat{\phi_g}(\mathcal{K})]$ and the variances $var[\widehat{h_v}(\mathcal{K})]$, $var[\widehat{\phi_g}(\mathcal{K})]$ of this estimation method. These values are shown in Figure 5 for Ex 1 with $h_v = 14.6\ m$ and in Figure 6 for Ex 3 with $h_v = 23.3\ m$ and with the linear polarization on transmit $P_{\pi/4}$ and with the worst one P_W for compact PolInSAR.

On the one hand, it can be observed that for large N values the estimator is approximatively efficient for both h_v and ϕ_g and for both transmit polarizations excepted for the estimation of h_v on Ex 1 with polarization P_W. It can also be noted that the bias is negligible for large N values for the estimated quantities.

On the other hand, for small N values, the estimations of h_v and ϕ_g can be biased with associated variances independent of N (the variance can be smaller than the CRB for biased estimators). The range of N for which the variances are constant is approximately the same for h_v and ϕ_g. Furthermore, this range is wider for the polarization P_W than for $P_{\pi/4}$.

It is possible to provide a simple interpretation of this phenomena (see appendix C). With small N values the region of coherence is badly estimated and the least squares line fits obtained with the different Jones vectors can have a uniformly distributed orientation between $-\pi$ and π for different realizations of $\mathcal{K}$. It can be shown that, in that case, a rough approximation (see appendix C) of the variance of $\widehat{\phi_g}(\mathcal{K})$ is

$$var^{sat}[\widehat{\phi_g}(\mathcal{K})] \simeq \frac{\arccos(a)^2}{3} \tag{18}$$

where a is the abscissa (i.e. real part) of the center of the coherence region after ground phase rotation. These values $var^{sat}[\widehat{\phi_g}(\mathcal{K})]$ have been reported for the considered examples in Figures 5 and 6 for polarizations P_W and $P_{\pi/4}$. It can be observed that it provides a good approximation of the maximal value of the variance of $\widehat{\phi_g}(\mathcal{K})$. The size N_s of the analyzed area under which the estimator is surely not efficient is therefore

$$N_s \simeq \frac{3\ CRB_1(\phi_g)}{\arccos(a)^2} \tag{19}$$

where $CRB_1(\phi_g)$ is the CRB for ϕ_g when $N = 1$.

These results show the relevance of the CRB analysis for the considered example even if a simple estimation method is implemented. They also emphasize the importance to implement compact PolInSAR with adapted transmit polarization.

V. Conclusion

In this paper, we have analyzed the loss of precision described by the Cramer-Rao Bound (CRB) in the vegetation height estimation when compact Polarimetric Interferometric Synthetic Aperture Radar (PolInSAR) is implemented instead of full PolInSAR. For that purpose, we have adapted the CRB methodology developed for P-band full PolInSAR in [1] to compact PolInSAR measurements. We have illustrated the approach with three examples chosen for their variability of polarimetric responses. Several observations result from this analysis. For these examples, the loss of precision can be small (smaller than a factor 2) for large set of transmit polarizations. However, for some transmit polarizations, this loss can be very large (about a factor 100). The precision described by the CRB is observed to be very dependent on the vegetation height when all the other parameters of the model are kept constant, with a factor greater than 100 in the CRB when h_v varies from $20m$ to $40m$ for two of the considered examples. This shows that the loss of precision considering Compact PolInSAR alternative with an appropriate incident polarization seems negligible in comparison to the influence of the vegetation height h_v. It has also been observed that the knowledge of the ground elevation can drastically improve the vegetation height precision by several orders of magnitude (more than a factor 100 has been observed).

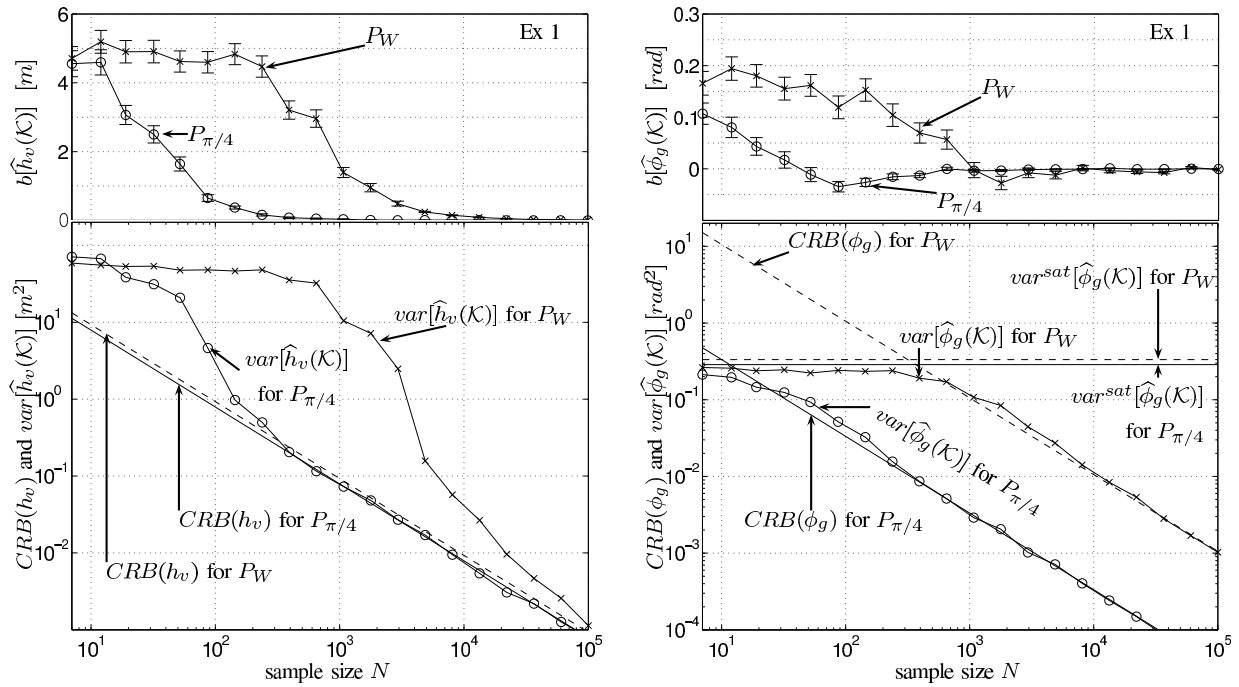

Fig. 5. Bias (upper curves) and variance (lower curves) of the estimation of h_v (left curves) and of ϕ_g (right curves) of the adapted Cloude and Papathanassiou estimator for the linear transmit polarization $P_{\pi/4}$ and the worst transmit polarization P_W as a function of the sample size N for Ex 1 and $h_v = 14.6\ m$. The bias and variances have been estimated on 500 independent realizations. The CRB have also been represented.

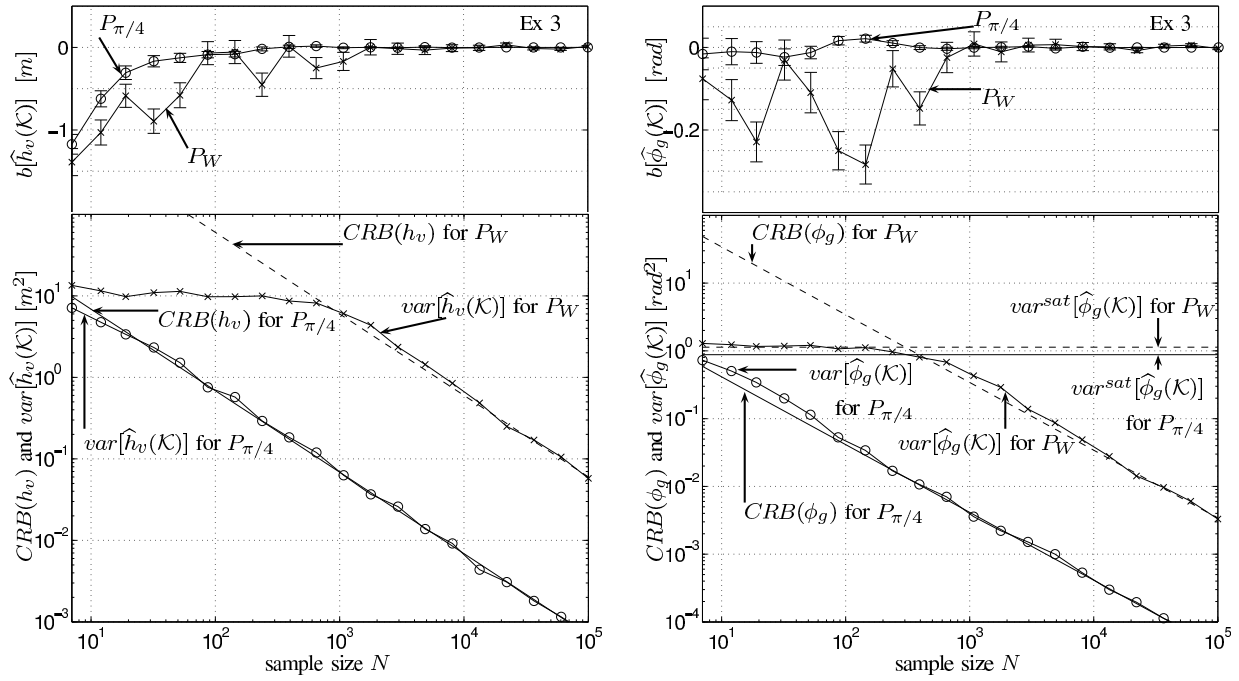

Fig. 6. The same as Fig.5 but for Ex 3 and $h_v = 23.3\ m$.

A straightforward estimation method such as the one introduced by Cloude and Papathanassiou [6] adapted to compact PolInSAR can lead to efficient estimation methods, i.e. unbiased and with a minimal variance equal to the CRB, for sufficiently large sets of pixels. Furthermore, a simple approximation has been proposed to determine the number of pixels under which the estimation is surely not efficient (i.e. does not reach the CRB). It has also been observed on the considered examples that, although the optimal transmit polarization depends on the vegetation height, the optimization of the transmit polarization for each possible vegetation height is not necessary to get acceptable performances. Moreover, circular, horizontal and $\pi/4$ transmit polarizations have lead to good performance, i.e. the CRB is degraded by a factor smaller than 5 on the considered examples while vertical transmit polarization can lead to a degradation by a factor 100.

This study demonstrates the relevance of the methodology based on the Cramer-Rao Bound to evaluate compact PolInSAR systems and missions. It also opens several motivating perspectives. Indeed, no proof has been provided in this paper that the observed behaviors apply to all physical situations characterized by different physical parameters such as the polarimetric coherency matrices $\boldsymbol{T}_{vol}$ and $\boldsymbol{T}_{gro}$. A better understanding of the key parameters influencing the values and the behavior of the CRB is an interesting challenge that should also allow one to get better physical insight in relation with the scattering mechanisms of the volume and forest grounds.

The effect of different sources of deviation to the simple considered homogeneous Random Vegetation over Ground model is also a worthwhile theme of research. In particular, since the precision described by the CRB is the minimal variance that can be obtained with unbiased estimators, the analysis of this paper provides a simple method to evaluate the confidence in practical estimations that can be useful to quantify the relative effect of other perturbation sources such as thermal noise, decoherence, non-homogeneous scatterer repartition. The analysis could be generalized to L-band or C-band. Releasing the Gaussian assumption might also be interesting for addressing large areas with non-uniform properties. Extension to multi-baselines PolInSAR systems is also very motivating since such systems can be powerful alternatives to get better precision, and a better description of forest structures and also to take into account temporal decorrelation which may occur with space-borne missions. Nevertheless, maybe the most direct perspective of this paper will be to evaluate if a fixed transmit polarization can be used so that an acceptable loss of precision can be obtained with compact PolInSAR in comparison with full PolInSAR for most of the realistic vegetation characteristics that would be analyzed with some space-borne missions.

Appendix A
Interpretation in the coherence disc

Let $\mathcal{D}_o$ denote the line in the plane that is determined with the region of coherence in the absence of fluctuations. Its equation can be written

$$x\ \cos(\theta) + y\ \sin(\theta) = d \tag{20}$$

where d is the distance between the line and the origin O of coordinates $(0,0)^T$ and θ is the angle between the line and the vertical axis. Let us assume that fluctuations due to the estimation with a finite set of pixels lead to the line $\mathcal{D}$ of equation

$$x\ \cos(\theta+\delta\theta) + y\ \sin(\theta+\delta\theta) = d + \delta d \tag{21}$$

such that this line corresponds to the rotation of $\mathcal{D}_o$ of angle $\delta\theta$ around the center O_R of the region of coherence of coordinates $(a_0, b_0)^T$. Since $O_R \in \mathcal{D}_o$ and $O_R \in \mathcal{D}$, assuming $\delta\theta \ll 1$, Eqs. 20 and 21 lead to

$$\delta d \simeq [b_0\ \cos(\theta) - a_0\ \sin(\theta)]\ \delta\theta \tag{22}$$

With the estimation method introduced in [6], fluctuations of z_g estimations correspond to fluctuations of θ. Ground phase correction corresponds to rotations of center O of $\mathcal{D}_o$ and $\mathcal{D}$. However, such rotations do not modify the distances of $\mathcal{D}_o$ and $\mathcal{D}$ to O which are thus respectively equal to d and $d+\delta d$. Since fluctuations of h_v estimations correspond to fluctuations of d, the fluctuations of z_g estimations do not imply fluctuations of h_v estimations if $\delta d = 0$ while $\delta\theta \neq 0$. Eq. 22 shows that such a situation occurs when $b_0\ \cos(\theta) - a_0\ \sin(\theta) = 0$, and thus when $(a_0, b_0) = \beta(\cos(\theta), \sin(\theta))$ where β is a real number. Introducing this result in Eq. 20 leads to

$$(a_0, b_0) = (d\ \cos(\theta), d\ \sin(\theta)) \tag{23}$$

In that case, see Fig. 7a., the angle between the segment $\overline{O, O_R}$ and the line $\mathcal{D}_o$ is equal to $\pi/2$. Ground phase correction transforms the line $\mathcal{D}_o$ into $\mathcal{D}'_o$ so that the point O_1 of coordinates $(1,0)$ belongs to $\mathcal{D}'_o$ (see Fig. 7.a). This rotation transforms O_R into

O'_R but the angle between the segments $\overline{O, O'_R}$ and $\overline{O'_R, O_1}$ is still equal to $\pi/2$, and thus O'_R is located on the circle of center $(1/2, 0)^T$ and of radius $1/2$.

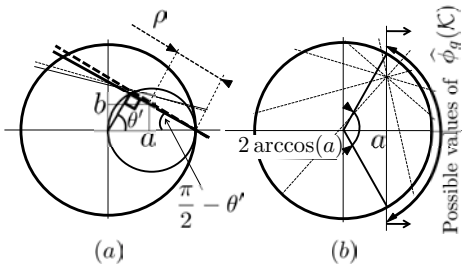

Fig. 7. (a): Schematic representation of the effect of an error in the estimation of z_g, and thus of the coherence line orientation. (b): Schematic representation of coherence line orientation variations on $\widehat{\phi_g}(\mathcal{K})$ at very low number of pixels N.

Appendix B
correlation and ratio of backscattered energies

An asymptotic region of coherence can be defined as the set of points in the complex plane defined by Eq. 16 but with the matrix $\widetilde{\boldsymbol{\Omega}}$, $\widetilde{\boldsymbol{T}}_1$ and $\widetilde{\boldsymbol{T}}_2$. It is well known [6] that

$$\gamma(\tilde{\boldsymbol{w}}) - 1 = \frac{\gamma_V - 1}{1 + r(\tilde{\boldsymbol{w}})} \tag{24}$$

where the ground phase is assumed equal to 0 and $\gamma_V = \gamma_V(h_v)$ is defined with Eq. 15, and with

$$r(\tilde{\boldsymbol{w}}) = \frac{a\ \tilde{\boldsymbol{w}}^\dagger \widetilde{\boldsymbol{T}}_{gro} \tilde{\boldsymbol{w}}}{I_1\ \tilde{\boldsymbol{w}}^\dagger \widetilde{\boldsymbol{T}}_{vol} \tilde{\boldsymbol{w}}} \tag{25}$$

When $r(\tilde{\boldsymbol{w}}) \simeq 1$, Eq. 24 leads to $\gamma(\tilde{\boldsymbol{w}}) - 1 \simeq (\gamma_V - 1)/2$. When $|\gamma_V| \simeq 1$, γ_V is near the circle of unit radius centered on $(0, 0)$. Thus, in that case, $\gamma(\tilde{\boldsymbol{w}})$ is near the circle of radius $1/2$ and centered on the point of coordinates $(1/2, 0)$. However, $r(\tilde{\boldsymbol{w}}) \simeq 1$ is equivalent to $a\ \tilde{\boldsymbol{w}}^\dagger \widetilde{\boldsymbol{T}}_{gro} \tilde{\boldsymbol{w}} \simeq I_1\ \tilde{\boldsymbol{w}}^\dagger \widetilde{\boldsymbol{T}}_{vol} \tilde{\boldsymbol{w}}$ which roughly corresponds to the situation for which the energy scattered by the ground is approximately equal to the energy that is scattered by the volume.

Appendix C
Saturation effect in the ϕ_g estimation

To get a simple interpretation of saturation effect in the ϕ_g estimation, and without loss of generality, let us assume that the true value of ϕ_g is equal to 0. For small N values, the least square line fit of the region of coherence can have a very fluctuating orientation and let us assume that this orientation is uniformly distributed between $-\pi$ and π. Since the estimated value $\widehat{\phi_g}(\mathcal{K})$ of ϕ_g corresponds to the intersection between the line and the complex circle which is the closest to the point $(1, 0)$, $\widehat{\phi_g}(\mathcal{K})$ varies between $-\arccos(a)$ and $\arccos(a)$ where a is this abscissa of the center of the coherence region (see Figure 7.b). With the above hypothesis the probability density function (pdf) of $\widehat{\phi_g}(\mathcal{K})$ can be determined but a simple rough approximation of the variance of $\widehat{\phi_g}(\mathcal{K})$ can be obtained assuming that this pdf is uniform between $-\arccos(a)$ to $\arccos(a)$ which leads to $var^{sat}[\widehat{\phi_g}(\mathcal{K})] \simeq \arccos(a)^2/3$.

Acknowledgment

Partial financial support for this work was provided by ONERA and CNES with a TOSCA program and the authors thank these last two institutions. The authors are grateful to Conseil Régional Provence-Alpes-Côte d'Azur (PACA) for taking part in the funding of the PhD of Aurélien Arnaubec. The authors would like to express their gratitude to the ONERA airborne radar team who is responsible for the radar acquisition and processing.

References

[1] A. Roueff, A. Arnaubec, P.-C. Dubois-Fernandez, and P. Réfrégier, "Cramer-Rao lower bound analysis of vegetation height estimation with random volume over ground model and polarimetric SAR interferometry," *IEEE Geosci. Remote Sens. Lett.*, vol. 8, no. 6, pp. 1115–1119, nov 2011.

[2] R. N. Treuhaft, S. Madsen, M. M., and van Zyl J.J., "Vegetation characteristics and underlying topography from interferometric data," *Radio Science*, vol. 31, pp. 1449–1495, nov-dec 1996.

[3] R. N. Treuhaft and P. Siqueira, "Vertical structure of vegetated land surfaces from interferometricand polarimetric radar," *Radio Science*, vol. 35, no. 1, pp. 141–177, jan-feb 2000.

[4] K. Papathanassiou and S. R. Cloude, "Single-baseline polarimetric SAR interferometry," *IEEE Trans. Geosci. Remote Sensing*, vol. 39, no. 11, pp. 2352–2363, nov 2001.

[5] T. Flynn, M. Tabb, and R. Carande, "Direct estimation of vegetation parameters from Covariance data in polarimetric SAR interferometry," in *Proc. IGARSS'02*. IEEE, 2002, pp. 1908–1910.

[6] S. Cloude and K. Papathanassiou, "Three-stage inversion process for polarimetric SAR interferometry," *IEEE Trans Radar Sonar Navigation*, vol. 150, no. 3, pp. 125–133, jun 2003.

[7] M. Tabb, T. Flynn, and R. Carande, "Full maximum likelihood inversion of PolInSAR scattering models," in *Proc. IGARSS'04*, no. 3. IEEE, 2004, pp. 1232–1235.

[8] F. Garestier, P. Dubois-Fernandez, and I. Champion, "Forest Height Inversion Using High-Resolution P-Band Pol-InSAR Data," *IEEE Trans. Geosci. Remote Sensing*, vol. 46, no. 11, Part 1, pp. 3544–3559, nov 2008.

[9] P. C. Dubois-Fernandez, J.-C. Souyris, S. Angelliaume, and F. Garestier, "The Compact Polarimetry Alternative for Spaceborne SAR at Low Frequency," *IEEE Trans. Geosci. Remote Sens.*, vol. 46, no. 10, Part 2, pp. 3208–3222, oct 2008.

[10] F. Garestier, P. C. Dubois-Fernandez, D. Guyon, and T. Le Toan, "Forest Biophysical Parameter Estimation Using L- and P-Band Polarimetric SAR Data," *IEEE Trans. Geosci. Remote Sens.*, vol. 47, no. 10, pp. 3379–3388, oct 2009.

[11] L. Ferro-Famil, M. Neumann, and Y. Huang, "Multi-baseline PolInSAR statistical techniques for the characterization of distributed media," in *Proc. IGARSS'09,* Cape Town, South Africa, 2009, pp. 971–974.

[12] M. Lavalle, D. Solimini, E. Pottier, and Y.-L. Desnos, "Compact polarimetric SAR interferometry," *Radar, Sonar Navigation, IET*, vol. 4, no. 3, pp. 449 –456, jun 2010.

[13] J. Souyris, P. Imbo, S. Fjortoft, R. Mingot, and L. J.S., "Compact polarimetry based on symmetry properties of geophysical media: The $\frac{\pi}{4}$ mode," *IEEE Trans. Geosci. Remote Sensing*, vol. 43, no. 3, pp. 634–646, mar 2005.

[14] R. Raney, "Dual-polarized SAR and Stokes parameters," *IEEE Geosci. Remote Sensing letters*, vol. 3, no. 3, pp. 317–319, jul 2006.

[15] M.-L. Truong-Loï, A. Freeman, P.-C. Dubois-Fernandez, and E. Pottier, "Estimation of Soil Moisture and Faraday Rotation from bare surfaces using compact polarimetry," *IEEE Trans. Geosci. Remote Sensing*, vol. 47, no. 11, pp. 3608–3615, nov 2009.

[16] S. Cloude, D. Goodenough, and H. Chen, "Compact decomposition theory," *Geoscience and Remote Sensing Letters, IEEE*, vol. 9, no. 1, pp. 28 –32, jan 2012.

[17] S. Nghiem, S. Yueh, R. Kwok, and F. Li, "Symmetry properties in polarimetric remote-sensing," *RADIO SCIENCE*, vol. 27, no. 5, pp. 693–711, sep-oct 1992.

[18] S. R. Cloude, *Polarisation: Applications in Remote Sensing*. New York: Oxford University Press, 2009.

[19] J. W. Goodman, *Speckle phenomena: Theory and Applications*. USA: Roberts & Company Publishers, 2006.

[20] J. S. Lee and E. Pottier, *Polarimetric Radar Imaging: from basics to applications*. USA: CRC Press, 2009.

[21] S. Huard, *Polarization of light*. Paris: Wiley, Masson, 1997.

[22] S. R. Cloude, "Polarization coherence tomography," *RADIO SCIENCE*, vol. 41, no. 4, aug 2006.

[23] M. Neumann, L. Ferro-Famil, and A. Reigber, "Estimation of Forest Structure, Ground, and Canopy Layer Characteristics From Multibaseline Polarimetric Interferometric SAR Data," *IEEE Transactions on Geoscience and Remote Sensing*, vol. 48, no. 3, Part 1, pp. 1086–1104, mar 2010.

[24] S. Tebaldini and F. Rocca, "Multibaseline Polarimetric SAR Tomography of a Boreal Forest at P- and L-Bands," *IEEE Transactions on Geoscience and Remote Sensing*, vol. 50, no. 1, pp. 232–246, jan 2012.

[25] R. Bamler and P. Hartl, "Synthetic aperture radar interferometry," *INVERSE PROBLEMS*, vol. 14, no. 4, pp. R1–R54, aug 1998.

[26] M. Tabb and R. Carande, "Robust inversion of vegetation structure parameters from low-frequency, polarimetric interferometric SAR," in *Proc. IGARSS'01*. IEEE, 2001, pp. 3188–3190.

[27] P. Garthwaite, I. Jolliffe, and B. Jones, *Statistical Inference*. London: Prentice Hall Europe, 1995.

[28] P. Stoica and R. Moses, *Spectral Analysis of Signals*. Prentice Hall, 2005.

[29] P. Dubois-Fernandez, T. Le Toan, S. Daniel, H. Oriot, J. Chave, L. Blanc, L. Villard, M. Davidson, and M. Petit, "The TropiSAR airborne campaign in French Guiana: Objectives, Description and Observed Temporal behavior of the Backscatter signal," *IEEE Trans. Geosci. Remote Sensing*, pp. 1–14, 2012.

[30] A. Freeman and S. L. Durden, "A three-component scattering model for polarimetric SAR data," *IEEE Trans. Geosci. Remote Sensing*, vol. 36, no. 3, pp. 963–973, 1998.

[31] A. Freeman, "Fitting a two-component scattering model to polarimetric SAR data from forests," *IEEE Transactions on Geoscience and Remote Sensing*, vol. 45, no. 8, pp. 2583–2592, aug 2007.

[32] J. David Ballester-Berman and J. M. Lopez-Sanchez, "Applying the Freeman-Durden Decomposition Concept to Polarimetric SAR Interferometry," *IEEE Transactions on Geoscience and Remote Sensing*, vol. 48, no. 1, pp. 466–479, jan 2010.

[33] C. Brosseau, *Fundamentals of polarized light - A statistical Optics approach*. New York: John Wiley, 1998.

[34] J.-J. Van Zyl, H.-A. Zebker, and C. Elachi, "Imaging RADAR polarization signatures - theory and observations," *Radio Science*, vol. 22, no. 4, pp. 529–543, 1987.

[35] S. Tebaldini, "Single and Multipolarimetric SAR Tomography of Forested Areas: A Parametric Approach," *IEEE Trans. Geosci. Remote Sens.*, vol. 48, no. 5, pp. 2375–2387, may 2010.

[36] O. Frey and E. Meier, "Analyzing Tomographic SAR Data of a Forest With Respect to Frequency, Polarization, and Focusing Technique," *IEEE Transactions on Geoscience and Remote Sensing*, vol. 49, no. 10, Part 1, SI, pp. 3648–3659, oct 2011.

[37] P. Réfrégier and F. Goudail, "Invariant polarimetric con-

trast parameters of coherent light," *J. Opt. Soc. Am. A*, vol. 19, no. 6, pp. 1223–1233, 2002.
[38] A. Arnaubec, A. Roueff, P.-C. Dubois-Fernandez, and P. Réfrégier, "Influence of the nature of a priori knowledge on the precision of vegetation height estimation in polarimetric SAR interferometry," in *EUSAR, Nuremberg, Germany*, 2012.

Aurélien Arnaubec received the Dipl.Ing. degree from the École Centrale Marseille, Marseille, France, in 2009. He received his Ph.D. degree when he was working on polarimetric and interferometric SAR at the French Aerospace Laboratory, Office National d'Etudes et Recherches Aérospatiales, (ONERA), Salon Cedex Air, France, and in the Physics and Image Processing Group, Fresnel Institute, Marseille, France. He is currently a research scientist in the IFREMER Underwater System Department. His research interests concern statistical signal processing.

Antoine Roueff received his Ph.D. from the Institut National Polytechnique de Grenoble (INPG) in 2003. From 2003 to 2005, he worked as a postdoctoral researcher at the Commissariat à l'Energie Atomique (CEA) in Paris. Since 2007 he is associate professor at Ecole Centrale de Marseille and does research at the Fresnel Institute. His research activity concerns the development of statistical analysis of multicomponent and multi-sensors signals. The application domains of his research are geophysics, optics and remote sensing.

Pascale C. Dubois-Fernandez received a Dipl.Ing. degree from « Ecole Nationale Supérieure d'ingénieur en constructions aéronautiques » France and a M's and Engineer's degrees from the California Institute of technology, Pasadena CA in 1983, 1984 and 1986, respectively. She joined the Radar science and technology group at the Jet Propulsion Laboratory, Pasadena, California where she stayed 10 years, participating in numerous programs like Magellan, AIRSAR, SIR-C. She then moved back to France, where she worked on cartographic applications of satellite data. In 2000, she joined ONERA, the French Aeronautics and Aerospace Research Institute as part of the Electromagnetism and Radar Department where she has been involved in the ONERA SAR airborne platforms, RAMSES, SETHI and BUSARD, developing the science applications as the SAR civilian remote sensing expert.

Philippe Réfrégier is presently professor at the Ecole Centrale de Marseille and member of the Fresnel Institute in which he is presently working on statistical optics, image processing and remote sensing. He has published two French books, two English books and more than 140 articles in international journals in optics, pattern recognition, statistical physics, image processing and remote sensing. He is OSA and EOS fellow.